

On the development of quasi-periodic oscillations in Bondi–Hoyle accretion flows

O. Dönmez,^{1*} O. Zanotti² and L. Rezzolla^{2,3}

¹*Department of Physics, Nigde University, Nigde 51200, Turkey*

²*Max-Planck-Institut für Gravitationsphysik, Albert Einstein Institut, Golm 14476, Germany*

³*Department of Physics, Louisiana State University, Baton Rouge, LA 70803, USA*

Accepted 2010 November 8. Received 2010 October 31; in original form 2010 October 4

ABSTRACT

The numerical investigation of the Bondi–Hoyle accretion on to a moving black hole has a long history, both in Newtonian and in general-relativistic physics. By performing new two-dimensional and general-relativistic simulations on to a rotating black hole, we point out a novel feature, namely that quasi-periodic oscillations (QPOs) are naturally produced in the shock cone that develops in the downstream part of the flow. Because the shock cone in the downstream part of the flow acts as a cavity trapping pressure perturbations, modes with frequencies in the integer ratios of 2:1 and 3:1 are easily produced. The frequencies of these modes depend on the black hole spin and on the properties of the flow, and scale linearly with the inverse of the black hole mass. Our results may be relevant for explaining the detection of QPOs in Sagittarius A*, once such detection is confirmed by further observations. Finally, we report on the development of the flip-flop instability, which can affect the shock cone under suitable conditions; such an instability has been discussed before in Newtonian simulations but was never found in a relativistic regime.

Key words: black hole physics – hydrodynamics – shock waves – Galaxy: disc hydrodynamics.

1 INTRODUCTION

Non-spherical accretion flows are astrophysically relevant in all those situations where strong winds with a small amount of angular momentum are able to transport considerable amounts of matter towards an accreting compact object, e.g. a black hole or a neutron star. Examples include the case of massive X-ray binaries in which a compact object accretes from the wind of an early-type star or the case of young stellar systems orbiting in the gravitational potential of their birth cluster and accreting from the dense molecular interstellar medium. One of the most celebrated and best-studied types of non-spherical accretion flows is the Bondi–Hoyle accretion flow (Hoyle & Lyttleton 1939; Bondi & Hoyle 1944) which, we recall, develops when a black hole moves relative to a uniform gas cloud. The Bondi–Hoyle flow has been the subject of several numerical investigations, starting from Matsuda, Inoue & Sawada (1987) and followed by Fryxell & Taam (1988), Sawada et al. (1989) and Benensohn, Lamb & Taam (1997). As a summary of the bulk of work done so far on this topic, table 1 of Foglizzo, Galletti & Ruffert (2005) reports an overview of published numerical simulations of the Bondi–Hoyle–Lyttleton accretion over the last 30 yr and lists more than 40 works. While providing detailed descriptions of the

morphology of the gas capture in the supersonic regime, several of the above-mentioned investigations were aimed at verifying the occurrence of the so-called flip-flop instability. This consists of an instability to tangential velocities of the shock cone that forms in the downstream region of the flow, and it manifests in the oscillation of the shock cone from one side to the other of the accretor.

In the relativistic regime, the first two-dimensional simulations of the Bondi–Hoyle accretion were performed by Petrich et al. (1989) and subsequently by Font & Ibáñez (1998b) and Font, Ibáñez & Papadopoulos (1998, 1999). These investigations considered flows both in axisymmetry and in the equatorial plane; interestingly, none of these works showed the occurrence of the flip-flop instability, so no evidence existed, prior to this work, of the development of the instability also in a curved space–time. More recently, a fully general-relativistic investigation of the Bondi–Hoyle accretion has been considered by Farris, Liu & Shapiro (2010) in the context of the merger of supermassive black hole binaries; in this case, however, no discussion of the flip-flop instability was presented.

However, the occurrence of the instability is not the only relevant physical process that may manifest in Bondi–Hoyle accretion flows. An additional one, which does not seem to have been considered so far, is related to the possibility that the shock cone traps oscillation modes, thus producing quasi-periodic oscillations (QPOs). The intuition is indeed simple yet rather suggestive. The typical shocked cone of the Bondi–Hoyle accretion is likely to provide a

*E-mail: odonmez@nigde.edu.tr

natural cavity for the development and confinement of oscillation modes of sonic nature. If the accretor is a compact object, Newtonian hydrodynamics is a good approximation only at large radial distances, while it can lead to misleading conclusions when studying the flow evolution close to the event horizon. In this paper, we perform two-dimensional general-relativistic hydrodynamics simulations by focusing on the dynamical behaviour of the Bondi–Hoyle shock cone under a wide range of parameters. The QPOs that we have found have typical frequencies in the range from 10^{-5} to 10^{-3} Hz for a black hole with $M = 10^6 M_\odot$ (and in the range from 1 to 10^2 Hz for a black hole with $M = 10 M_\odot$). As a result, they can become relevant for the interpretation of QPOs observed both in the Galactic Centre and in high-mass X-ray binaries (HMXBs). Our analysis has also shown that the flip-flop instability does occur even in the relativistic framework, and we have investigated how such instability can interplay with the QPO phenomenon, by suppressing or exciting specific modes of oscillations.

The plan of the paper is as follows. In Section 2 we provide an overview of the hydrodynamical equations, of the numerical methods adopted and of the physical set-up of the problem. In Section 3 we describe our results, while Section 4 contains a discussion of the potential applicability to two specific astrophysical cases. Finally, Section 5 is devoted to the conclusions of our work. We use a geometrized system of units with $G = c = 1$.

2 MATHEMATICAL FORMULATION

2.1 General-relativistic hydrodynamics equations

We study the Bondi–Hoyle accretion of a perfect fluid in the curved background space–time of a rotating black hole. The energy–momentum tensor of the fluid has the usual form

$$T^{\mu\nu} = h\rho u^\mu u^\nu + pg^{\mu\nu}, \quad (1)$$

where u^μ is the 4-velocity of the fluid and h , ρ and p are the specific enthalpy, the rest-mass density and the pressure, respectively. All of these quantities are measured by an observer comoving with u^μ , while $g^{\mu\nu}$ is the metric of the space–time. By adopting the 3 + 1 formalism of general relativity and after choosing Boyer–Lindquist coordinates (t, r, θ, ϕ) , the line element of the metric is written as

$$ds^2 = -\left(1 - \frac{2Mr}{\Sigma^2}\right) dt^2 - \frac{4Mar}{\Sigma^2} \sin^2\theta dt d\phi \\ + \frac{\Sigma^2}{\Delta} dr^2 + \Sigma^2 d\theta^2 + \frac{A}{\Sigma^2} \sin^2\theta d\phi^2,$$

where

$$\Sigma^2 \equiv r^2 + a^2 \cos^2(\theta), \quad (2)$$

$$\Delta \equiv r^2 - 2Mr + a^2, \quad (3)$$

$$A \equiv (r^2 + a^2)^2 - a^2 \Delta \sin^2\theta, \quad (4)$$

with a and M being the spin and the mass of the black hole, respectively. The *lapse* function and the *shift* vector of the metric are given, respectively, by $\alpha = (\Sigma^2 \Delta / A)^{1/2}$ and $\beta^i = (0, 0, -2Mar/A)$. When solving numerically the general-relativistic hydrodynamic equations, it is important to write them in a conservation form (Banyuls et al. 1997):

$$\frac{\partial \mathbf{U}}{\partial t} + \frac{\partial \mathbf{F}^i}{\partial q^i} = \mathbf{S}. \quad (5)$$

where \mathbf{U} , \mathbf{F}^i and \mathbf{S} are the vectors of the conserved variables, of the fluxes and of the sources, respectively, while q^i is the generalized coordinate in the i th direction. When performing two-dimensional numerical simulations in the equatorial plane, equation (5) reduces to

$$\frac{\partial \mathbf{U}}{\partial t} + \frac{\partial \mathbf{F}^r}{\partial r} + \frac{\partial \mathbf{F}^\phi}{\partial \phi} = \mathbf{S}. \quad (6)$$

The conservative variables, written in terms of the primitive variables (ρ, v^i, p) , are

$$\mathbf{U} = \begin{bmatrix} D \\ S_r \\ S_\phi \\ \tau \end{bmatrix} = \begin{bmatrix} \sqrt{\gamma} W \rho \\ \sqrt{\gamma} \rho h W^2 V_r \\ \sqrt{\gamma} \rho h W^2 V_\phi \\ \sqrt{\gamma} (\rho h W^2 - p - W\rho) \end{bmatrix}, \quad (7)$$

where $V^i = u^i / W + \beta^i / \alpha$ is a spatial vector whose indices are raised and lowered through the spatial metric γ_{ij} and it represents the 3-velocity of the fluid with respect to the Eulerian observer associated with the 3 + 1 splitting of the metric. $W = (1 - \gamma_{ij} V^i V^j)^{-1/2}$ is the Lorentz factor of the fluid and $\gamma = \det(\gamma_{ij}) = \Sigma^4 \sin^2\theta / \alpha^2$ is the determinant of 3-metric. Although Font et al. (1999) already reported fluxes and sources for the hydrodynamical equations in the Kerr metric, we explicitly list them here for convenience as

$$\mathbf{F}^r = \begin{bmatrix} \alpha(V^r - \beta^r/\alpha)D \\ \alpha\{(V^r - \beta^r/\alpha)S_r + \sqrt{\gamma}p\} \\ \alpha(V^r - \beta^r/\alpha)S_\phi \\ \alpha\{(V^r - \beta^r/\alpha)\tau + \sqrt{\gamma}V^r p\} \end{bmatrix}, \quad (8)$$

$$\mathbf{F}^\phi = \begin{bmatrix} \alpha(V^\phi - \beta^\phi/\alpha)D \\ \alpha(V^\phi - \beta^\phi/\alpha)S_r \\ \alpha\{(V^\phi - \beta^\phi/\alpha)S_\phi + \sqrt{\gamma}p\} \\ \alpha\{(V^\phi - \beta^\phi/\alpha)\tau + \sqrt{\gamma}V^\phi p\} \end{bmatrix} \quad (9)$$

and

$$\mathbf{S} = \begin{bmatrix} 0 \\ \alpha\sqrt{\gamma}T^{\mu\nu}g_{\nu\sigma}\Gamma_{\mu r}^\sigma \\ \alpha\sqrt{\gamma}T^{\mu\nu}g_{\nu\sigma}\Gamma_{\mu\phi}^\sigma \\ \alpha\sqrt{\gamma}\left(T^{rt}\partial_r\alpha - \alpha\left(T^{rt}\Gamma_{rt}^t + T^{rr}\Gamma_{rr}^t + T^{r\phi}\Gamma_{r\phi}^t\right)\right) \end{bmatrix}. \quad (10)$$

The equation of state that we adopt is that of an ideal gas, namely $p = (\Gamma - 1)\rho\epsilon$,

where Γ and ϵ are the adiabatic index and the specific internal energy, respectively. The reference adiabatic index used in the simulations is $\Gamma = 4/3$, though we have also considered different values to explore the effect on the results.

We have solved the system of equation (5) through high-resolution shock-capturing schemes based on approximate Riemann solvers. A *minmod* linear algorithm for the reconstruction of the left and right states at each interface between adjacent numerical cells is adopted, while the numerical fluxes are computed with the Marquina flux formula. More specific details about the numerical scheme can be found in Dönmez (2004).

As a final remark we note that because we are not considering here any contribution coming from the cooling of the shocked gas, the oscillations we will discuss are not related to those reported by Molteni, Sponholz & Chakrabarti (1996), Chakrabarti, Acharyya & Molteni (2004) and Okuda, Teresi & Molteni (2007). In those studies, in fact, the presence of cooling processes is a necessary ingredient for the appearance of oscillations along the standing shocks.

Table 1. Initial models adopted in numerical simulation. From left to right, the columns are the name of the model, the black hole spin a , the asymptotic flow velocity V_∞ , the asymptotic Mach number \mathcal{M}_∞ and the inner boundary r_{in} of the grid. The final simulation time is set equal to $10\,000M$ in all of the models. The reference adiabatic index adopted is $\Gamma = 4/3$, though we have also considered different values to explore the effect on the results.

Model	a/M	V_∞	\mathcal{M}_∞	$r_{\text{in}}(M)$
A1	0.9	0.001	0.01	1.78
A2	0.9	0.1	1	1.78
A3	0.9	0.2	2	1.78
A4	0.9	0.3	3	1.78
A5	0.9	0.4	4	1.78
A6	0.9	0.5	5	1.78
A7	0.9	0.6	6	1.78
<i>B</i>	0.5	0.4	4	2.1
C1	0.0	0.001	0.01	2.1
C2	0.0	0.1	1	2.1
C3	0.0	0.2	2	2.1
C4	0.0	0.3	3	2.1
C5	0.0	0.4	4	2.1
C6	0.0	0.5	5	2.1
C7	0.0	0.6	6	2.1

2.2 Initial conditions, boundary conditions and approximations

We perform numerical simulations on the equatorial plane, i.e. $\theta = \pi/2$. The initial velocity field is given in terms of an asymptotic velocity V_∞ as in Font et al. (1998), i.e.

$$V^r = \sqrt{\gamma^{rr}} V_\infty \cos(\phi), \quad (12)$$

$$V^\phi = -\sqrt{\gamma^{\phi\phi}} V_\infty \sin(\phi). \quad (13)$$

These relations guarantee that the velocity of the injected gas at infinity is parallel to the x -direction, while $V^2 \equiv V_i V^i = V_\infty^2$ everywhere in the flow. The value of V_∞ can then be chosen to investigate the different regimes of the flow and to consider therefore subsonic or supersonic accretion.

During the evolution additional matter is injected supersonically from the outer boundary in the upstream region with the same analytic prescription of (12) and (13), thus reproducing a continuous wind at large distances. The initial density and pressure profiles are adjusted to make the sound speed equal to a required value, which we choose to be $c_{s,\infty} = 0.1$. In practice, once $c_{s,\infty}$ is chosen, we set the density to be a constant (i.e. $\rho = 1$) and then the pressure is derived from the relativistic definition of the sound speed, i.e. $p = c_{s,\infty}^2 \rho (\Gamma - 1) / [\Gamma(\Gamma - 1) - c_{s,\infty}^2 \Gamma]$. A brief description of the initial models is reported in Table 1, where model C* refers to Schwarzschild black holes and different fluid injection velocities, while models A* and B refer to Kerr black holes, respectively, with spin $a/M = 0.9$ and 0.5 , again spanning different fluid injection velocities.

The computational grid consists of $N_r \times N_\phi$ uniformly spaced zones in the radial and angular directions, respectively, covering a computational domain extending from r_{min} (reported in Table 1) to $r_{\text{max}} = 43M$ and from 0 to 2π . For our fiducial simulation we have chosen $N_r = 512$ and $N_\phi = 256$, but have also verified that the qualitative results (i.e. the appearance of the QPOs or of the instability) are not sensitive to the resolution used or to the location

of the outer boundary, which has been moved to $r_{\text{max}} \simeq 80M$ in some tests.

The boundary conditions in the radial direction are such that at the inner radial grid point, we implement outflow boundary conditions by a simple zeroth-order extrapolation (i.e. a direct copy) of all variables. At the outer radial boundary, on the other hand, we must distinguish between the upstream region, with $\pi/2 < \phi < 3/2\pi$, and the downstream region, with $-\pi/2 < \phi < \pi/2$. In the upstream region we continuously inject matter with the initial velocity field, while in the downstream region we use outflow boundary conditions. Finally, periodic boundary conditions are adopted along the ϕ direction.

Finally, we note that in order to validate the code, we have carried out a number of comparisons with the ECHO code presented in Del Zanna et al. (2007), which, among other differences, uses a non-uniform grid structure. The results obtained from the two codes have not shown significant differences.

3 NUMERICAL RESULTS

3.1 Properties of the stationary pattern

The main features of the Bondi–Hoyle accretion were first investigated in the relativistic framework through a number of numerical simulations by Petrich et al. (1989), Font & Ibáñez (1998b) and Font et al. (1998, 1999). The overall results obtained can be summarized as follows.

As already shown by several authors, when a homogeneous flow of matter moves non-radially towards a compact object, a shock wave will form in the neighbourhood of the accretor. Depending then on the properties of the flow, namely on the adiabatic index and on the asymptotic Mach number \mathcal{M}_∞ , the shock can either reach very close to the accretor or be at a certain distance from it (see e.g. Foglizzo et al. 2005). More specifically, for any given value of \mathcal{M}_∞ , there is a critical adiabatic index $\Gamma \simeq 2$, below which a shock wave of conic shape, i.e. a ‘shock cone’, forms in the downstream part of the flow, i.e. downstream of the accretor. Matter from the upstream region continuously crosses the shock front, undergoes a strong deceleration and, if it is inside the accretion radius, is ultimately accreted. As a result, the maximum rest-mass density in the downstream region is always larger than the corresponding one in the upstream region and, consequently, the mass accretion rate is significantly non-spherical and larger in the downstream part of the flow. Interestingly, when suitable coordinates are used (e.g. Kerr–Schild coordinates), it has been shown by Font et al. (1999) that the shock even penetrates the event horizon. On the other hand, for increasingly stiff fluids and thus for values of the adiabatic index larger than the critical one, a bow-shock wave forms in the upstream part of the flow, i.e. upstream of the accretor. In this case the accretion is almost spherical and because the bow shock does not reach into the black hole’s horizon, it is often referred to as a ‘detached’ shock.

The shape of the shock cone depends sensitively on the spin of the black hole. If the black hole is not spinning, then the shock cone is perfectly symmetric at $\phi = 0$. On the other hand, if the black hole is spinning, the induced frame-dragging effect produces a ‘wrapping’ of the shock cone, as already shown and discussed in great detail by Font et al. (1999).

Our simulations essentially confirm this picture, and the main features of the stationary pattern are summarized in Figure 1, which shows the two-dimensional rest-mass density distribution (left-hand panel) and the Lorentz factor distribution (right-hand panel) for

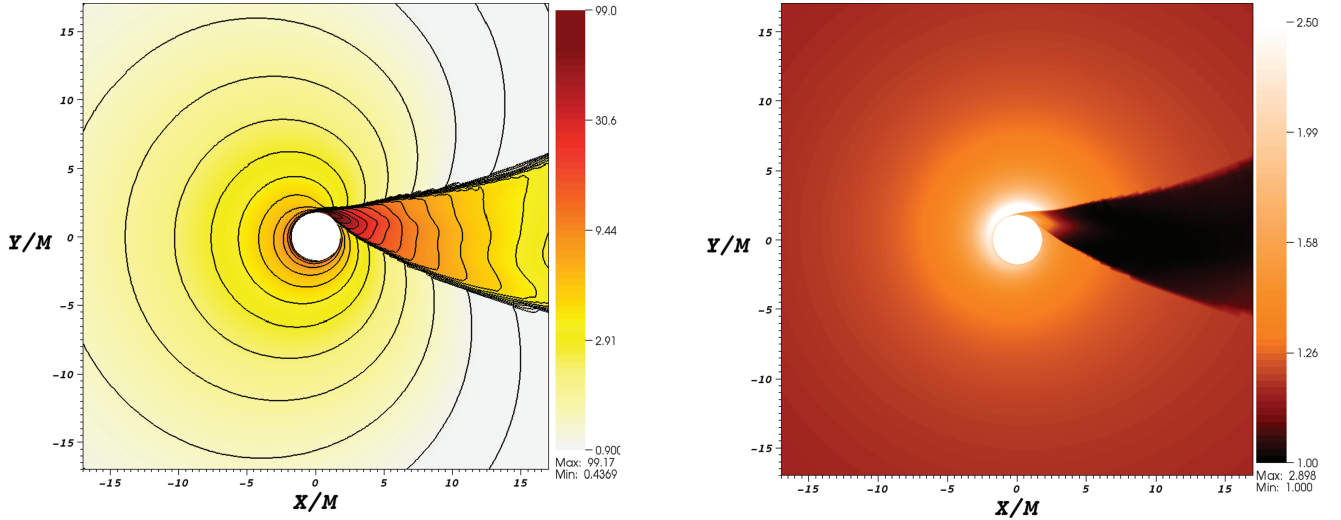


Figure 1. Rest-mass density distribution (left-hand panel) and Lorentz factor distribution (right-hand panel) for a black hole with spin $a = 0.9$ and a supersonic flow with asymptotic velocity $V_\infty = 0.5$, and at time $t = 10000 M$. In the downstream region, a clear shock cone forms which is distorted by the non-vanishing spin of the black hole.

model A6 with $a/M = 0.9$ and $V_\infty = 0.5$. As evident from the iso-density contours, the accretion in the upstream region is essentially spherical accretion, while a very well-defined shock cone, characterized by a strong density gradient, forms in the downstream region. The shock cone, where the accretion rate is the largest, is clearly distorted by the spin of the black hole and its opening angle slightly decreases with an increasing distance from the centre. We have also found that spinning black holes have maximum rest-mass density in the shock cone which is higher than for non-spinning black holes. The right-hand panel of Fig. 1, on the other hand, shows that the overall flow is only very mildly relativistic, with a maximum Lorentz factor $W_{\max} \lesssim 3$, even ahead of the shock front in the vicinity of the black hole. It is also interesting to note that accretion in the shock cone takes place with a very small Lorentz factor. Matter inside the shock cone can accrete on to the black hole

only for radii smaller than a given *accretion radius* r_a , defined as the radius where the accretion rate (as a function of radius) becomes negative. The expression $r_a \approx 2M/(V_\infty^2 + c_{s,\infty}^2)$, which is valid in the case of a purely spherical accretion, provides a good estimate of the accretion radius in the Bondi–Hoyle accretion. As an example, for a model with $V_\infty = 0.5$ and $c_{s,\infty} = 0.1$, we found $r_a = 6.1$, while the predicted one is $r_a = 7.6$.

To complement the information in Fig. 1, Fig. 2 shows one-dimensional profiles at time $t = 10000 M$ of the rest-mass density at different radial shells for an asymptotic flow velocity $V_\infty = 0.5$. More specifically, the left-hand panel refers to a Schwarzschild black hole, while the right-hand panel to a rotating black hole with spin $a/M = 0.9$. Clearly, a sharp transition in the density exists at the border of the shock cone and this is particularly evident for the non-rotating black hole. Note also the amount of distortion which

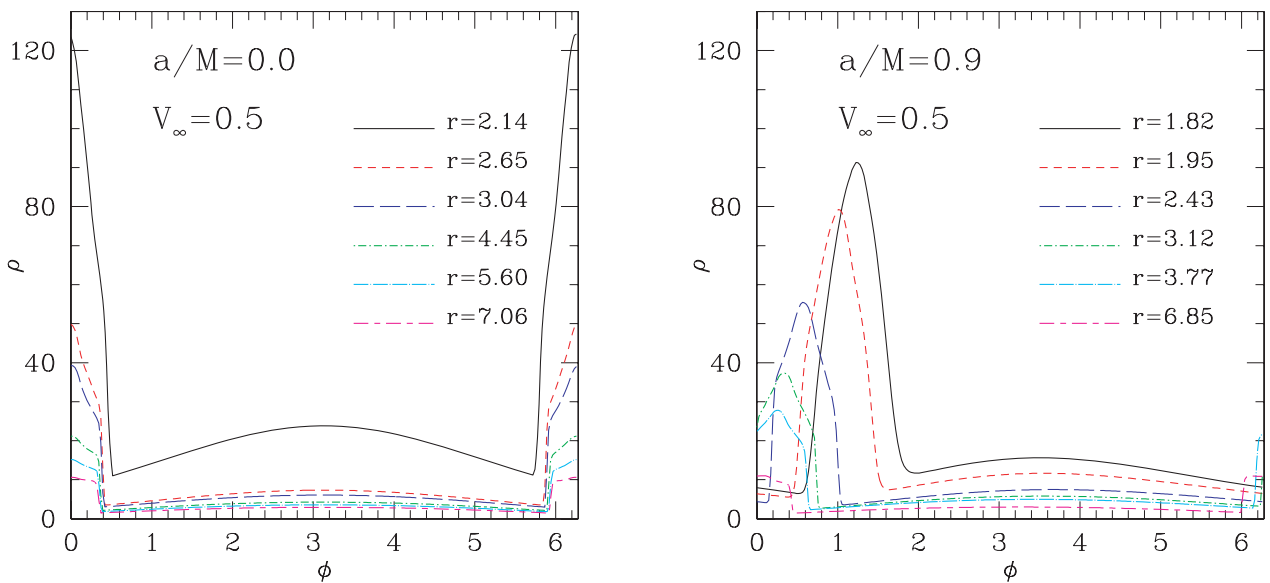


Figure 2. One-dimensional profiles of the rest-mass density at time $t = 10000 M$, showing the location of the shock at different radial shells for an asymptotic flow velocity $V_\infty = 0.5$. The left-hand panel refers to a Schwarzschild black hole, while the right-hand panel to a rotating black hole with spin $a/M = 0.9$. Note that in this latter case, the shock is distorted and no longer symmetric.

is present in the case of a rotating black hole; although this is in part due to our choice of Boyer–Lindquist coordinates, similar distortions are present also when using different and better suited coordinates, such as Kerr–Schild [see the discussion in Font et al. (1999)]. As already mentioned above, the angular location of the shock is only weakly dependent on the radial distance, with the size of the shock cone reducing only slightly when moving away from the black hole. As a final remark, we note that the large degree of symmetry shown in the left-hand panel of Fig. 2 provides a convincing evidence of the abilities of the code to maintain the symmetry across $\phi = 0$.

3.1.1 The flip-flop instability

As shown through numerical simulations performed by several authors over the years in Newtonian physics, the Bondi–Hoyle accretion flow is subject to the so-called *flip-flop* instability, namely an instability of the shock cone to tangential velocities, which manifests in the oscillation of the shock cone from one side of the accretor to the other. Such instability was first discovered by Matsuda et al. (1987) in two-dimensional Newtonian axisymmetric simulations, and later confirmed and further investigated by Fryxell & Taam (1988), Sawada et al. (1989), Benensohn et al. (1997), Foglizzo & Ruffert (1999) and Pogorelov, Ohsugi & Matsuda (2000). Three-dimensional simulations were performed by Ishii et al. (1993) and Ruffert (1997), who confirmed the occurrence of the instability, although with deformations of the shock cone only very close to the accretor. In spite of all these investigations, however, the nature and the physical origin of the flip-flop instability remain obscure. According to Foglizzo & Ruffert (1999), for example, local instabilities, such as the Rayleigh–Taylor or the Kelvin–Helmholtz instabilities, should not play a significant role and cannot account for the flip-flop instability. On the other hand, Soker (1990) showed, through a WKB analysis, that the two-dimensional axisymmetric accretion flow (not the one considered in our work) can be unstable against tangential modes as well as against radial modes. When extending these results to three-dimensional simulations, however, the persistence of such instabilities is not fully clarified. Overall, it is fair to say that, although the flip-flop instability has been confirmed numerically in both two- and three-dimensional simulations, it is still unclear whether the physical mechanisms driving the instabilities in the two cases are the same or not. Finally, to further complicate the scenario, no evidence was found by Font et al. (1998) of such an instability within a relativistic framework, although the authors argued that an instability might develop for very large values of the asymptotic Mach number.

More recently, Foglizzo et al. (2005) performed a very detailed analysis of the unstable behaviour of Bondi–Hoyle accretion flows, suggesting that the instability may be of advective-acoustic nature, in the case of shocks both attached and detached (bow shocks) to the accretor. Moreover, they also stressed that, though physical, the instability is likely to be triggered or dumped by numerical effects such as the carbuncle phenomenon at the shock, the boundary condition at the surface of the accretor and the grid size.

Although a detailed analysis of the flip-flop instability is beyond the scope of this paper, which is rather focused on the development of QPOs in Bondi–Hoyle accretion flows, our simulations confirm for the first time the occurrence of the instability even in a relativistic regime. Fig. 3, for instance, reports four snapshots of the rest-mass density in a long-term evolution of a model when the instability is fully developed. The shock cone in the downstream region oscillates

back and forth in the orbital plane in this representative model with black hole spin $a/M = 0.5$ and $V_\infty = 0.4$. The reason why such unstable behaviour was not noticed by Font et al. (1999) may be due to the short-term evolution that they were forced to consider at the time or, as suggested by Foglizzo et al. (2005), because of the high values of $2M/r_a = (V_\infty^2 + c_{s,\infty}^2)$ that they considered.

Fig. 4 shows additional key features of the flip-flop instability. The top panel, in particular, reports the shock-opening angle, as a function of the asymptotic velocity, computed in radians at $r = 4.43M$ and $t = 10\,000M$. Shown with different lines are the values for a Schwarzschild black hole (red solid line) and for a Kerr black hole (blue dashed line). The points with $V_\infty = 0.3$ and 0.4 correspond to models which are flip-flop unstable and are located close to the local maximum of the shock-opening angle. This result confirms what was already reported by Livio et al. (1991), namely that the instability manifests when the shock-opening angle is larger than a given threshold. Once the instability is fully developed, the mass accretion rate experiences high amplitude oscillations (for any value of the spin considered). This is shown in the bottom panel of Fig. 4, reporting the evolution of the one-dimensional mass accretion rate \dot{M} defined as

$$\dot{M} \equiv - \int_0^{2\pi} \alpha \sqrt{\gamma} \rho W \left(v^r - \frac{\beta^r}{\alpha} \right) d\phi, \quad (14)$$

for different choices of V_∞ ; the specific values reported in the figure refer to a shell at $r = 6.08M$ and a rotating black hole with spin $a/M = 0.9$. It is therefore evident that for small values of V_∞ , both the mass accretion rate and the shock-opening angle are increasing functions of V_∞ . However, the accretion is no longer efficient above a critical value of $V_\infty \simeq 0.4$, and any further increase in V_∞ causes both the accretion rate and the maximum rest-mass density in the shock cone to decrease.

3.2 QPOs in the shock cone

As mentioned in Section 1, one of the most important results presented in this work is about the development of QPOs in the shock cone that forms in the downstream region once the system has relaxed to the stationary state. Note that because a stationary state is necessary for the development of the QPOs, the latter are not found when the flip-flop instability develops. Although the occurrence of QPOs in the Bondi–Hoyle accretion has not been discussed before in previous numerical investigations, fig. 8 of Font & Ibáñez (1998a) does show a clear periodic behaviour of the accretion rate. So, although we can claim to be the first ones to have pointed out the appearance of this effect and to have investigated it in detail, we cannot claim to be the first to have shown found it from numerical simulations.

In order to extract as much information as possible about the emerged phenomenology and provide a first physical explanation, we have carried out an extensive Fourier analysis of the different dynamical quantities. The two panels of Fig. 5, for instance, show the power spectra obtained from the time series of the rest-mass density as computed in a region which is in the middle of the shock cone for a flow with asymptotic velocity $V_\infty = 0.1$. The left-hand and right-hand panels refer to black holes with spins for $a/M = 0.0$ and 0.9 , respectively, while the mass is the same in the two cases and equal to $M = 10 M_\odot$. The different curves refer to time series recorded at different radial positions but have the same azimuthal position. After performing a series of tests at different resolutions, we have estimated the error bar in the measure of each frequency to be ~ 3 Hz.

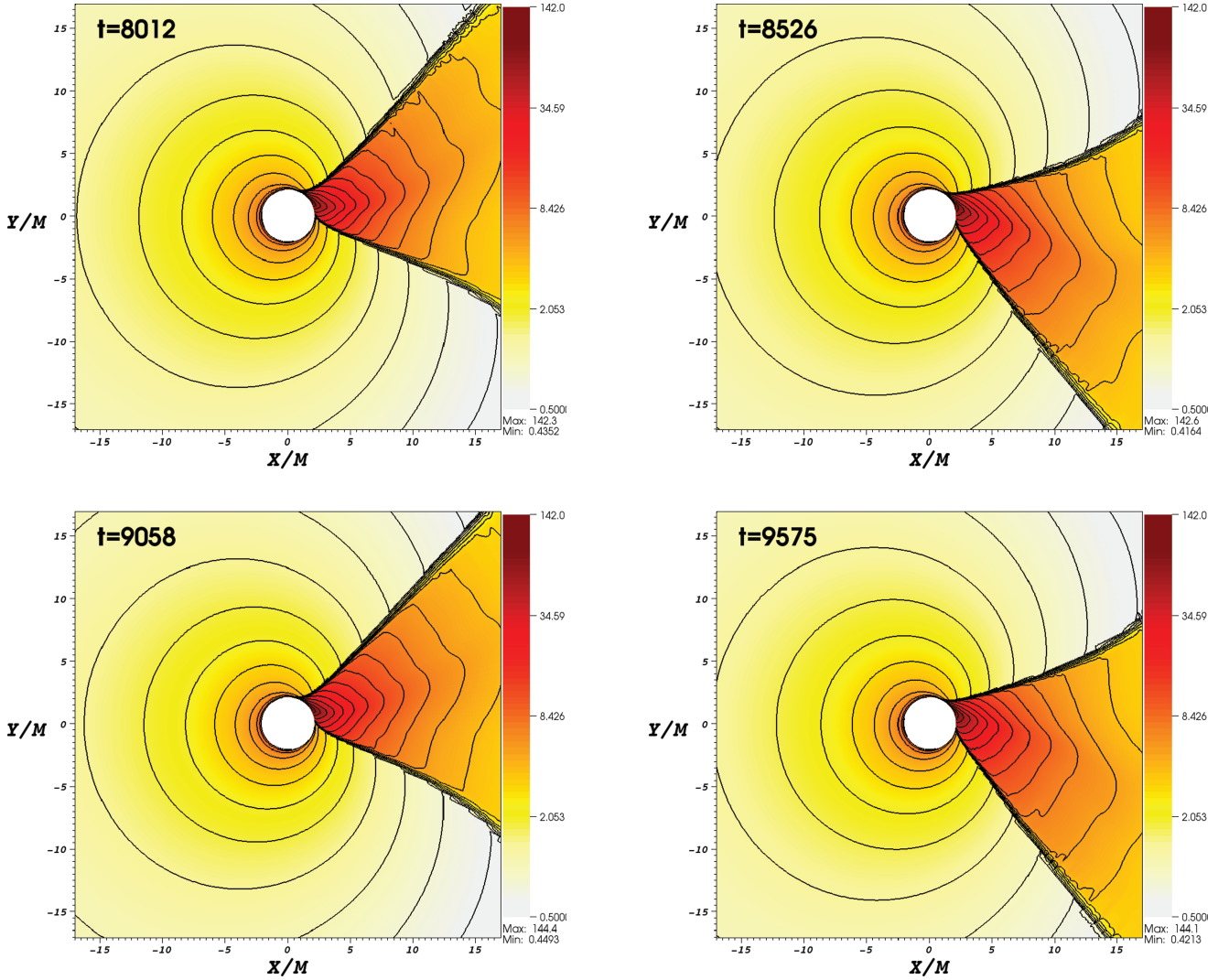


Figure 3. Logarithm of the density at different times for model *B* with $a/M = 0.5$ and $V_\infty = 0.4$. The flip-flop instability manifests after the shock cone has reached a stationary state, and it causes the shock cone to oscillate back and forth with an oscillation period around $1046M$.

A number of comments should be made regarding the spectra reported in Fig. 5. The first one is that the modes of oscillation are essentially independent of the radial position, i.e. the power spectra at different radii overlap extremely well. This is a clear indication that the modes are local waves but they are global eigenmodes of the system.

The second comment is that, among the modes reported in Fig. 5, some are genuine eigenmodes, while others are simply the result of non-linear couplings. In particular, the modes with frequencies $f_1 = 21$ Hz and $f_2 = 34$ Hz in the left-hand panel of Fig. 5 are genuine eigenmodes, while those at 55, 68, 83 and 106 Hz are given, within a few per cent error, by non-linear couplings of the eigenmodes, i.e. $f_1 + f_2$, $2f_2$, $3f_2 - f_1$ and $3f_2$, respectively. Similarly, the modes $f_1 = 40$ Hz and $f_2 = 64$ Hz in the right-hand panel of Fig. 5 are genuine eigenmodes, while the modes at 81, 104 and 124 Hz are given, within few per cent errors, by $2f_1$, $f_1 + f_2$ and $3f_1$, respectively. We recall that this behaviour is typical of physical systems governed by non-linear equations in the limit of small oscillations (Landau & Lifshitz 1976) and has already been pointed out by Zanotti et al. (2005) in the context of oscillation modes in thick accretion discs around black holes. It should also be remarked that, while a large

number of modes due to non-linear coupling exists, the identification becomes difficult for frequencies larger than 100 Hz. Similarly, the low-frequency mode at ~ 5 Hz, which is visible in both the panels of Fig. 5, could be a genuine mode but it appears with much smaller intensity and not all radii. As a result, its classification as a genuine mode will require more accurate simulations and on much longer time-scales.

The global nature of the oscillation modes inside the shock cone is clearly shown in Fig. 6, which represents the power spectral intensity of the most powerful mode in the right-hand panel of Fig. 5, namely of the mode at $f = 124$ Hz (A very similar behaviour can be seen in the case of a non-rotating black hole.) In other words, for each grid cell inside the shock cone we store the evolution of the rest-mass density and compute from this the power spectral density. We then consider a single frequency and study how its intensity is distributed (in arbitrary units) inside the shock cone.

Note that the intensity is computed over the whole computational domain, but it has a non-negligible amplitude only inside the shock cone, and this amplitude becomes increasingly stronger near the black hole. (We recall that in general we do not expect the amplitude to be constant in the shock cone, as this depends on the specific

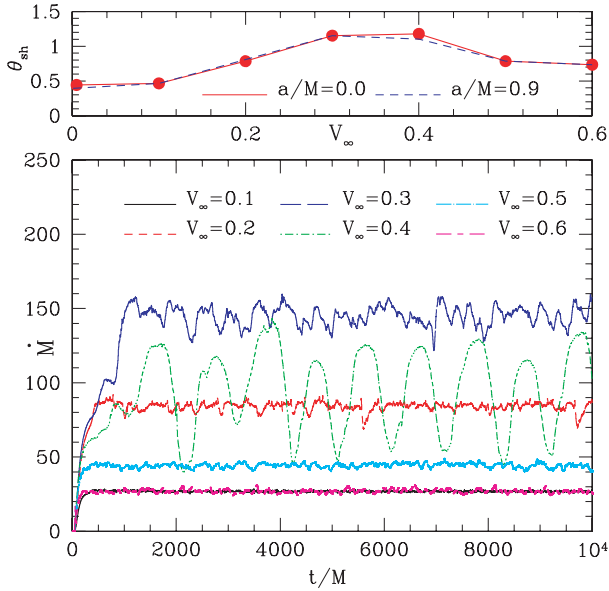


Figure 4. Top panel: shock-opening angle in radians as computed at $r = 4.43M$, $t = 10000M$, as a function of V_∞ . Shown with different lines are the values for a Schwarzschild black hole (red solid line) and for a Kerr black hole (blue dashed line). Bottom panel: time evolution of the mass accretion rate, computed at $r = 6.08M$, for different values of V_∞ and a rotating black hole with spin $a/M = 0.9$. The mass accretion rate manifests high amplitude oscillation in the two flip-flop unstable models with $V_\infty \sim 0.3$ – 0.4 .

eigenfunction of the mode.) What is shown in Fig. 6 is not specific to the mode at $f = 124$ Hz, and we have verified that the spatial distribution of the intensity manifests a similar pattern for all of the other modes. Besides providing evidence that these are indeed global oscillation modes of the flow, Fig. 6 also highlights that QPOs can be excited in the shock cone of a Bondi–Hoyle-type accretion and that these are stronger close to the black hole.

Interestingly, when the flip-flop instability is triggered and develops, the power spectra inside the shock cone change considerably and in these cases only the periodicity of the shock-cone oscillation can be found, which is then accompanied by the usual non-linear

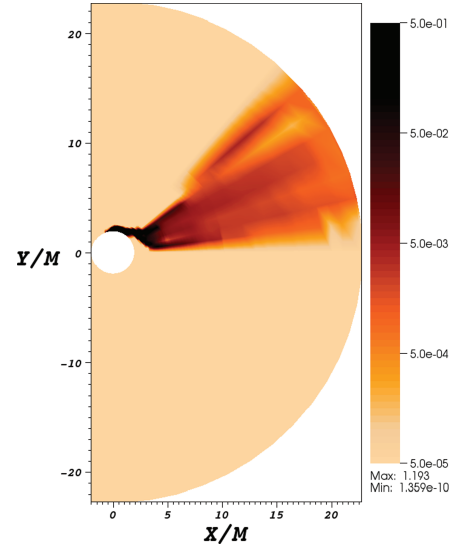


Figure 6. Spatial distribution of the power spectral density at $f = 124$ Hz for a black hole of mass $M = 10 M_\odot$ and spin $a/M = 0.9$ (cf. right-hand panel of Fig. 5). A very similar behaviour would be shown in the case of a non-rotating black hole.

couplings. In general, therefore, the effect of the flip-flop instability is that of suppressing most of the internal modes of oscillations. A more detailed analysis of this process as well as of the flip-flop instability will be presented in a future work.

A linear perturbative analysis of the stationary pattern would certainly be of great interest for three important reasons: first, in order to identify unambiguously which of the modes are genuine (or fundamental) and which are the effect of non-linear coupling; secondly, to compute the expected eigenfrequencies and eigenfunctions of the oscillations we have discovered numerically; and finally to clarify why some modes are more efficiently excited than others. However, such perturbative analysis is probably going to be extremely complicated, mainly because of the absence of an analytic solution for the stationary flow inside the shock cone. To counter these limitations and perform a first rudimentary analysis of the eigenfunctions, we report in Fig. 7 a map of what can be regarded

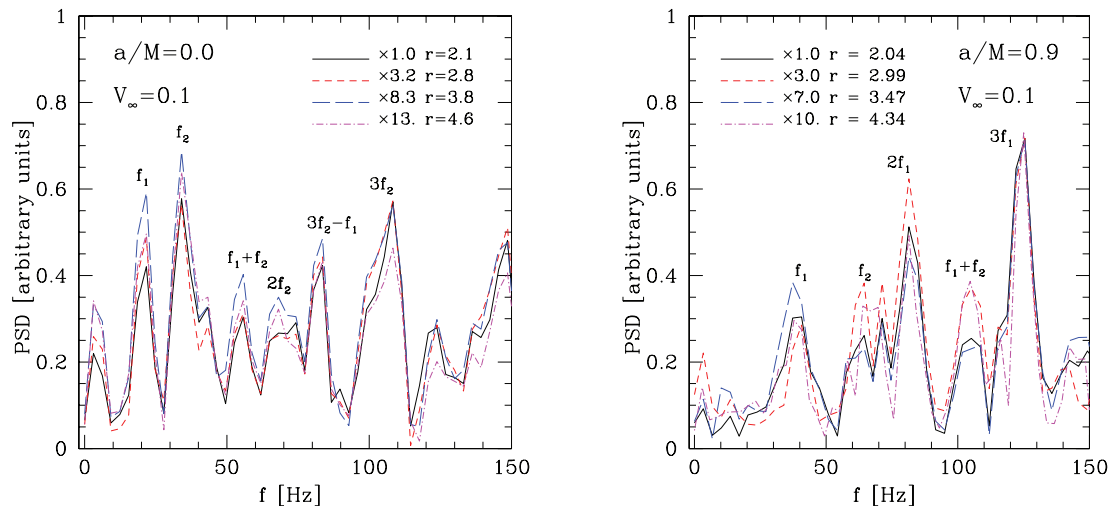


Figure 5. Power spectra of the time series of the rest-mass density as computed at the centre of a shock cone for a flow with asymptotic velocity $V_\infty = 0.1$. The left-hand and right-hand panels refer to black holes with spins for $a/M = 0.0$ and 0.9 , respectively, while the mass is the same in the two cases and $M = 10 M_\odot$. The different curves refer to time series recorded at different radial positions but have the same azimuthal position.

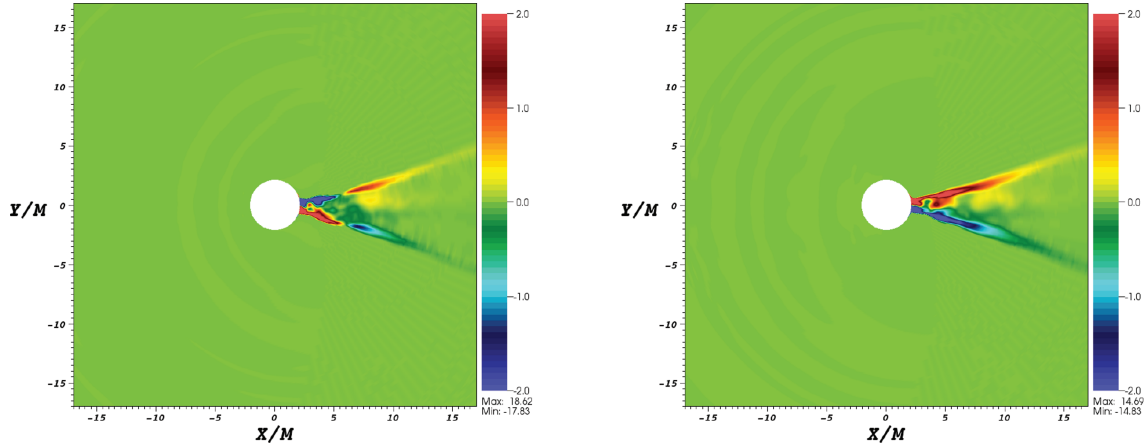


Figure 7. Numerical eigenfunctions computed as $\rho(r, \phi) - \bar{\rho}_0(r, \phi)$, where $\bar{\rho}_0(r, \phi)$ is the density distribution when the flow is stationary (i.e. for $t \gtrsim 1500M$). The left-hand and right-hand panels report two snapshots at $t = 1871M$ and $2162M$, respectively, and are separated by half a period of oscillation; both refer to a black hole with spin $a/M = 0.0$ and $V_\infty = 0.1$.

Table 2. Frequencies of the first two genuine modes measured within the shock cone from the evolution of the rest-mass density. The values refer to different black hole spins and different asymptotic velocities, while the mass of the black hole is always assumed to be $M = 10 M_\odot$. Note that the frequencies scale linearly with M and the values reported have an error bar of ~ 3 Hz.

a/M	V_∞	f_1 (Hz)	f_2 (Hz)
0.0	0.1	21	34
0.5	0.1	32	53
0.9	0.1	40	64
0.0	0.2	32	46
0.9	0.2	46	84

as a numerical eigenfunction for the model C2 ($V_\infty = 0.1$ and spin $a/M = 0.0$). In fact, the two panels of Fig. 7 show the difference $\rho(r, \phi) - \bar{\rho}_0(r, \phi)$, where $\bar{\rho}_0(r, \phi)$ is the density distribution when the flow is stationary (i.e. for $t \gtrsim 1500M$). Considering, for example, the left-hand panel, which corresponds to $t = t_1 = 1871M$ and using Cartesian coordinates, we show in the upper part of the figure that, i.e. for $y/M > 0$, the density perturbation along the shock is negative close to the black hole, while it is positive far from it. A specular behaviour is detected in the lower part of the figure where $y/M < 0$. The computed perturbation oscillates in time with a given period P , and the right-hand panel of the figure shows a snapshot at time $t_2 = t_1 + P/2 = 2162M$, i.e. at half a period of oscillation. Although heuristic, this procedure allows us to compute the period of oscillation of the perturbation with a very good accuracy. The corresponding frequency, again computed assuming $M = 10 M_\odot$, is, in fact, $f \sim 35$ Hz and it matches very well with the most powerful mode, that with frequency f_2 , reported in the left-hand panel of Fig. 5. To highlight the dependence of the eigenfrequencies on the black hole spin, we report in Table 2 their values as measured within the shock cone from the evolution of the rest-mass density. The mass of the black hole is assumed to be $M = 10 M_\odot$, but the frequencies can be easily computed for an arbitrary mass since they scale linearly with the black hole mass. The data in Table 2 suggest that a linear scaling is also present for the black hole spin, but

clearly more data are necessary to confirm this scaling, which we will investigate in a future work.

As a final remark we note that, overall, the phenomenology we have found shows strong similarities with that reported for perturbed relativistic tori orbiting around a black hole (Zanotti, Rezzolla & Font 2003). In that case, it was shown by Rezzolla, Yoshida & Zanotti (2003b) through a perturbative investigation that the eigenfunctions and eigenfrequencies were those corresponding to the p modes of the torus. Such modes, also known as inertial-acoustic waves, are closely related to the propagation of sound waves in the perturbed fluid and have pressure gradients and centrifugal forces as the main restoring forces. The major difference of the physical conditions investigated by Rezzolla et al. (2003b) with the ones considered here is that centrifugal forces play a negligible role in Bondi–Hoyle accretion flows. Apart from this, however, the physical nature of the modes is essentially the same in the two cases. When applied to the oscillations of a thick disc around a compact object, such modes motivated the proposal of a model for explaining the detection of high-frequency quasi-periodic oscillations in the spectra of X-ray binaries (Rezzolla et al. 2003a).

4 ASTROPHYSICAL APPLICATIONS

4.1 The case of Sgr A*

A possible application of the results discussed in the previous section and, in particular, of the development of QPOs in the downstream part of a Bondi–Hoyle flow is offered by the source Sagittarius A* (or Sgr A*). Such a source is located at the centre of our Galaxy and is widely believed to be a supermassive black hole with an estimated mass of $\sim 4.1 \pm 0.6 \times 10^6 M_\odot$ (Ghez et al. 2008; Gillessen et al. 2009). Sgr A* is one of the most intensely observed astronomical objects, and the phenomenology of its emission is both rich and particularly complex. Interestingly, however, QPOs from its emission have been observed by Aschenbach et al. (2004) (see also Aschenbach 2009), when analysing two distinct near-infrared and X-ray flares (Genzel et al. 2003). In particular, Aschenbach et al. (2004) reported five different peaks at periods of 100, 219, 700, 1150 and 2250 s in the power spectral density of such flares. Soon after, Abramowicz et al. (2004) noted that $(1/700):(1/1150):(1/2250) \approx 3:2:1$, that is, the periods are in a harmonic ratio. Indeed, while discussing the same source, Török

(2005) confirmed the measurement of a double peak of QPOs in Sgr A* in the same typical 3:2 ratio observed in several low-mass X-ray binaries and suggested the epicyclic resonance model by Abramowicz et al. (2003) as a possible explanation for this phenomenon. Chan et al. (2009), on the other hand, performed two-dimensional magnetohydrodynamical simulations of a putative accretion disc in Sgr A* and showed that the QPO frequencies could be due to non-axisymmetric density perturbations, and which may be used to set a lower limit on the orbital period at the innermost stable circular orbit.

In addition to QPOs, Sgr A* is likely to have a Bondi–Hoyle accretion flow. This possibility was first pointed out by Melia (1992), who, after looking at the broad He I, Br α and Br γ emission lines, inferred that there is a strong circumnuclear wind near the dynamical centre of the Galaxy. In this scenario, the central black hole is assumed to be fed by stellar winds within several arcseconds from the compact object (Shcherbakov & Baganoff 2009). In order to investigate this possibility further, Ruffert & Melia (1994) performed the first three-dimensional hydrodynamical simulations of this system and computed the line-integrated flux assuming that the emission is dominated by bremsstrahlung. By collecting information coming from more recent observations, Cuadra et al. (2006) and Cuadra & Nayakshin (2006) performed smoothed particle hydrodynamics simulations of wind accretion on to Sgr A*, including optically thin radiative cooling and finding, among other results, that most of the accreted gas is hot and has a nearly stationary accretion rate. Although the observed luminosity is some orders of magnitude smaller than what is predicted by the Bondi–Hoyle model, this may be due to a low radiative efficiency of the accretion flow rather than to a failure of the Bondi–Hoyle model itself.

Should the two observational features mentioned above be confirmed by additional and more accurate observations, there would be a unique astronomical realization of a source for which both QPOs and Bondi–Hoyle accretion are simultaneously present. It should be stressed that the typical length-scale at which the QPOs develop in our simulations is $\approx 20M$, which thus corresponds to $\approx 4 \times 10^{-6}$ pc for the estimated mass of Sgr A*. This length-scale is much smaller than the closest approach to the Galactic Centre of the closest star S16, which is around $\approx 2 \times 10^{-4}$ pc, as reported by Ghez et al. (2005). Therefore, the Bondi–Hoyle accretion flow that could potentially be present in Sgr A*, would take place in a gas-dominated region very close to the central black hole and far from the orbits of the S-stars.

Interestingly, after analysing recent data about a high-level X-ray activity of Sgr A* observed with *XMM-Newton* (Porquet et al. 2008; Aschenbach 2009), Aschenbach (2009) reports nine prominent peaks, named ν_1, \dots, ν_9 . Out of these, only three are identified as fundamental, namely ν_6, ν_7 and ν_9 , while the other six are obtained as linear combinations of the fundamental ones, like, for instance, $\nu_6 + \nu_7, \nu_6 + \nu_9, \nu_7 - \nu_9$. Aschenbach (2009) interprets the three fundamental modes in terms of orbital, radial epicyclic and vertical epicyclic frequencies, respectively. In doing so, a specific radius where the oscillation is excited must be provided, the above oscillation frequencies being intrinsically local. On the contrary, no radial specification is required within our interpretation, since the modes are global and just confined within the shock cone. Finally, although Aschenbach (2009) does not give any explanation for the other six modes, they are however naturally provided within our interpretation of a Bondi–Hoyle accretion in which the downwind shock cone acts as a cavity, generating a whole series of non-linear couplings among few genuine and trapped pressure modes.

4.2 QPOs in HMXBs

A second application of our result is in principle represented by QPOs observed in the spectra of HMXBs, which are composed of a compact object and of an early-type (OB) star. The catalogue by Liu, van Paradijs & van den Heuvel (2006) lists 114 HMXB candidates in the Galaxy, some of which are believed to contain a black hole, such as Cyg X-1, NGC 5204 (Liu, Bregman & Seitzer 2004), M33 X-7 (Pietsch et al. 2004) and M101 ULX-1 (Mukai et al. 2005). Because in these systems the accretion flow occurs preferentially in the form of an accretion wind rather than in the form of an accretion disc, the Bondi–Hoyle accretion flow has been traditionally considered very relevant for them [see the review by Edgar (2004) for the application of the Bondi–Hoyle solution to binary systems]. However, the QPOs that have been detected in HMXBs have frequencies that are seen to lie in the range of 1–400 mHz, with the remarkable exception of XTE J0111.2–7317, which shows a QPO feature at 1.27 Hz (Kaur et al. 2007). On the other hand, the QPOs we have computed assuming a black hole of mass $M = 10M_{\odot}$ have frequencies which lie in the range from 1 to 500 Hz, and therefore that overlap only marginally with the observed ones.

5 CONCLUSIONS

Although viscous accretion discs represent the most natural channel by means of which compact objects accrete large amounts of matter with significant angular momentum, non-spherical accretion flows appear in all those situations in which the accreting matter has only a modest amount of angular momentum, such as in winds. The Bondi–Hoyle accretion is the most representative example of this type of flow and its study via numerical investigation has a long history, both in Newtonian and in general-relativistic physics. We have reconsidered this old problem by performing new two-dimensional and general-relativistic simulations on to a rotating black hole. Besides recovering many of the features of this flow which were discussed by other authors over the years, we have also pointed out a novel feature. More specifically, we have shown that under rather generic conditions a shock cone develops in the downstream region of the flow and that such a cone acts like a cavity trapping pressure modes and giving rise to QPOs.

These modes are global in the sense that they represent harmonic oscillations across the cavity, but have amplitudes that are larger in the region very close to the black hole, i.e. for $r \lesssim 10M$. While the black hole spin influences the absolute frequencies of the trapped modes, which lie in the range from 1 to 500 Hz for a representative black hole of mass $M = 10M_{\odot}$, it does not affect the fact that they appear in a series of integer numbers 1:2:3. This is because non-linear coupling of modes is common in systems governed by non-linear equations, and once a mode is excited, all of its integer multiples are also excited, thus producing a wide range of possible ratios of integer numbers.

In addition to pointing out this novel feature of the Bondi–Hoyle accretion, we have discussed its possible application to the phenomenology reported in Sgr A*, where both QPOs (Aschenbach et al. 2004) and Bondi–Hoyle accretion (Melia 1992) are likely to be present. Remarkably, a large family of linear combinations of modes have been recently identified by Aschenbach (2009) after analysing data about a high-level X-ray activity of Sgr A* observed with *XMM-Newton* (Porquet et al. 2008). This phenomenology could indeed be interpreted in terms of a shock cone that behaves

like a cavity and that generates a whole class of non-linear coupling among pressure modes.

Finally, we have provided the first evidence for the occurrence in a general-relativistic context of the so-called flip-flop instability of a Bondi–Hoyle flow. More specifically, we have shown that for a fixed choice of the black hole spin and of the sound speed, there exists a critical value of the asymptotic flow velocity at which the shock cone undergoes large-scale and coherent oscillations. When this happens, the opening angle of the shock cone reaches its maximum value, the accretion rate increases considerably and is no longer stationary. A more comprehensive analysis is needed to clarify the physical nature of the instability and its dynamics in the relativistic regime. This will be the focus of a future work.

Finally, among the future improvements of our work we plan to investigate the effects of a magnetic field, which is certainly likely to play a role but whose effective contribution has not been considered yet in numerical simulations of Bondi–Hoyle accretion flows. In particular, the potential interplay of the magnetorotational instability (MRI) with the flip-flop instability has to be taken into account, though it is not clear whether a local instability such as the MRI can substantially affect a global instability. As far as the occurrence of QPOs is concerned, on the other hand, we believe that it will remain essentially unchanged. The reason for this is that as long as a shock cone forms in the downstream part of the flow, QPOs will be naturally excited and trapped, the only difference being that they will be of magnetosonic nature rather than of a sonic one, and hence with eigenfrequencies that will depend not only on the properties of the shock cone (and thus of the fluid) but also on the strength of the magnetic field.

ACKNOWLEDGMENTS

It is a pleasure to thank José A. Font for carefully reading the manuscript and for very helpful comments. The numerical calculations were performed at the National Center for High Performance Computing of Turkey (UYBHM) under grant number 10022007 and TUBITAK ULAKBIM, High-Performance and Grid-Computing Center (TR-Grid e-Infrastructure). This work was supported in part by the DFG grant SFB/Transregio 7.

REFERENCES

- Abramowicz M. A., Karas V., Kluzniak W., Lee W. H., Rebusco P., 2003, *PASJ*, 55, 467
 Abramowicz M. A., Kluzniak W., McClintock J. E., Remillard R. A., 2004, *ApJ*, 609, L63
 Aschenbach B. E., 2009, preprint (arXiv:0911.2431)
 Aschenbach B., Grosso N., Porquet D., Predehl P., 2004, *A&A*, 417, 71
 Banyuls F., Font J. A., Ibáñez J. M., Martí J. M., Miralles J. A., 1997, *ApJ*, 476, 221
 Benensohn J. S., Lamb D. Q., Taam R. E., 1997, *ApJ*, 478, 723
 Bondi H., Hoyle F., 1944, *MNRAS*, 104, 273
 Chakrabarti S. K., Acharyya K., Molteni D., 2004, *A&A*, 421, 1
 Chan C.-k., Liu S., Fryer C. L., Psaltis D., Özel F., Rockefeller G., Melia F., 2009, *ApJ*, 701, 521

- Cuadra J., Nayakshin S., 2006, *J. Phys. Conf. Ser.*, 54, 436
 Cuadra J., Nayakshin S., Springel V., Di Matteo T., 2006, *MNRAS*, 366, 358
 Del Zanna L., Zanotti O., Bucciantini N., Londrillo P., 2007, *A&A*, 473, 11
 Dönmez O., 2004, *Ap&SS*, 293, 323
 Edgar R., 2004, *New Astron. Rev.*, 48, 843
 Farris B. D., Liu Y. T., Shapiro S. L., 2010, *Phys. Rev. D*, 81, 084008
 Foglizzo T., Ruffert M., 1999, *A&A*, 347, 901
 Foglizzo T., Galletti P., Ruffert M., 2005, *A&A*, 435, 397
 Font J. A., Ibáñez J. M., 1998a, *MNRAS*, 298, 835
 Font J. A., Ibáñez J. M., 1998b, *ApJ*, 494, 297
 Font J. A., Ibáñez J. M., Papadopoulos P., 1998, *ApJ*, 507, L67
 Font J. A., Ibáñez J. M., Papadopoulos P., 1999, *MNRAS*, 305, 920
 Fryxell B. A., Taam R. E., 1988, *ApJ*, 335, 862
 Genzel R., Schödel R., Ott T., Eckart A., Alexander T., Lacombe F., Rouan D., Aschenbach B., 2003, *Nat*, 425, 934
 Ghez A. M., Salim S., Hornstein S. D., Tanner A., Lu J. R., Morris M., Becklin E. E., Duchêne G., 2005, *ApJ*, 620, 744
 Ghez A. M. et al., 2008, *ApJ*, 689, 1044
 Gillessen S., Eisenhauer F., Trippe S., Alexander T., Genzel R., Martins F., Ott T., 2009, *ApJ*, 692, 1075
 Hoyle F., Lyttleton R. A., 1939, in *Proc. Cambridge Philosophical Society Vol. 35, The Effect of Interstellar Matter on Climatic Variation*. Cambridge Univ. Press, Cambridge, p. 405, doi:10.1017/50305004100021150
 Ishii T., Matsuda T., Shima E., Livio M., Anzer U., Boerner G., 1993, *ApJ*, 404, 706
 Kaur R., Paul B., Raichur H., Sagar R., 2007, *ApJ*, 660, 1409
 Landau L. D., Lifshitz E. M., 1976, *Mechanics*, Vol. 1. Pergamon Press, Oxford
 Liu J., Bregman J. N., Seitzer P., 2004, *ApJ*, 602, 249
 Liu Q. Z., van Paradijs J., van den Heuvel E. P. J., 2006, *A&A*, 455, 1165
 Livio M., Soker N., Matsuda T., Anzer U., 1991, *MNRAS*, 253, 633
 Matsuda T., Inoue M., Sawada K., 1987, *MNRAS*, 226, 785
 Melia F., 1992, *ApJ*, 387, L25
 Molteni D., Sponholz H., Chakrabarti S. K., 1996, *ApJ*, 457, 805
 Mukai K., Still M., Corbet R. H. D., Kuntz K. D., Barnard R., 2005, *ApJ*, 634, 1085
 Okuda T., Teresi V., Molteni D., 2007, *MNRAS*, 377, 1431
 Petrich L. I., Shapiro S. L., Stark R. F., Teukolsky S. A., 1989, *ApJ*, 336, 313
 Pietsch W., Mochejska B. J., Misanovic Z., Haberl F., Ehle M., Trinchieri G., 2004, *A&A*, 413, 879
 Pogorelov N. V., Ohsugi Y., Matsuda T., 2000, *MNRAS*, 313, 198
 Porquet D. et al., 2008, *A&A*, 488, 549
 Rezzolla L., Yoshida S., Maccarone T. J., Zanotti O., 2003a, *MNRAS*, 344, L37
 Rezzolla L., Yoshida S., Zanotti O., 2003b, *MNRAS*, 344, 978
 Ruffert M., 1997, *A&A*, 317, 793
 Ruffert M., Melia F., 1994, *A&A*, 288, L29
 Sawada K., Matsuda T., Anzer U., Boerner G., Livio M., 1989, *A&A*, 221, 263
 Shcherbakov R. V., Baganoff F. K., 2010, *ApJ*, 716, 504
 Soker N., 1990, *ApJ*, 358, 545
 Török G., 2005, *A&A*, 440, 1
 Zanotti O., Rezzolla L., Font J. A., 2003, *MNRAS*, 341, 832
 Zanotti O., Font J. A., Rezzolla L., Montero P. J., 2005, *MNRAS*, 356, 1371

This paper has been typeset from a $\text{\TeX}/\text{\LaTeX}$ file prepared by the author.